Neurochemistry International 87 (2015) 1–12

Contents lists available at ScienceDirect

Neurochemistry International

journal homepage: www.elsevier.com/locate/nci

SWATH analysis of the synaptic proteome in Alzheimer's disease

Rachel Yoon Kyung Chang, Naomi Etheridge, Amanda S. Nouwens, Peter R. Dodd *

School of Chemistry and Molecular Biosciences, University of Queensland, Australia

ARTICLE INFO

Article history:
Received 9 February 2015
Received in revised form 20 April 2015
Accepted 21 April 2015
Available online 6 May 2015

Keywords:
Human
Proteomics
HPLC
Cerebral cortex
Pathway analysis
Cellular assembly and organization

ABSTRACT

Brain tissue from Alzheimer's disease patients exhibits synaptic degeneration in selected regions. Synaptic dysfunction occurs early in the disease and is a primary pathological target for treatment. The molecular mechanisms underlying this degeneration remain unknown. Quantifying the synaptic proteome in autopsy brain and comparing tissue from Alzheimer's disease cases and subjects with normal aging are critical to understanding the molecular mechanisms associated with Alzheimer pathology. We isolated synaptosomes from hippocampus and motor cortex so as to reduce sample complexity relative to whole-tissue homogenates. Synaptosomal extracts were subjected to strong cation exchange (SCX) fractionation to further partition sample complexity; each fraction received SWATH-based information-dependent acquisition to generate a comprehensive peptide-ion library. The expression of synaptic proteins from AD hippocampus and motor cortex was then compared between groups. A total of 2077 unique proteins were identified at a critical local false discovery rate <5%. Thirty of these, including 17 novel proteins, exhibited significant expression differences between cases and controls; these proteins are involved in cellular functions including structural maintenance, signal transduction, autophagy, oxidative stress, and proteasome activity, or they have synaptic-vesicle related or energy-related functions. Differentially expressed proteins were subjected to pathway analysis to identify protein–protein interactions. This revealed that the most perturbed molecular and cellular functions were cellular assembly and organization. Core analysis revealed RhoA signaling to be the top canonical pathway. Network analysis showed that differentially expressed proteins were related to cellular assembly and organization, and cellular function and maintenance. This is the first study to combine SCX fractionation with SWATH analysis. SWATH is a promising new technique that can greatly enhance protein identification in any proteome, and has many other benefits; however, there are limitations yet to be resolved.

1. Introduction

The pathological hallmarks of Alzheimer's disease (AD) are intracellular neurofibrillary tangles, extracellular amyloid plaques, and neuronal loss. The pathology is region-specific: the hippocampus is severely affected whereas occipital and motor cortices are relatively spared (Honer et al., 1992). Increasing evidence suggests that locally severe synaptic dysfunction and neuronal degeneration, which are observed in parts of the AD brain (DeKosky and Scheff, 1990; Honer et al., 1992), may underlie disease progression. The degree of degeneration strongly correlates with the deterioration of cognitive abilities ante mortem (DeKosky and Scheff, 1990). However, the molecular mechanisms that lead to synaptic loss are unclear.

Subcellular fractionation prior to proteomic analysis allows the assay of less-abundant proteins by reducing sample complexity. Previous studies have quantified proteins in synaptosomal (Chang et al., 2013), nuclear (Ren et al., 2014), cytosolic (Tremblay et al., 2011), and mitochondrial fractions (Shi et al., 2008) from human autopsy brain. Using two-dimensional (2D) gel electrophoresis on human brain synaptosome extracts, we identified 1000 and ~1700 proteins in separate studies (Chang et al., 2013; Etheridge et al., 2009); these numbers include isoforms and proteins with post-translational modification (PTM). Liquid chromatography (LC) separation with tandem mass spectrometry (MS/MS) allowed over 1400 proteins to be quantified in whole brain tissue (Andreev et al., 2012). These numbers are low, considering that over 3000 proteins are currently estimated to occur in human synaptic endings, excluding isoforms and PTM forms (Grant, 2006).

Multiple reaction monitoring (MRM), in which proteotypic peptides of a protein of interest are targeted, is highly sensitive and reproducible for protein quantification by MS/MS. Ions within a narrow range of mass to charge ratio (m/z) values around that of the target precursor ion are transmitted in the first mass spectrometer quadrupole. The precursor ion is fragmented in the second quadrupole by collision-induced dissociation, and the third quadrupole then transmits ions in a narrow m/z range around those of

* Corresponding author. School of Chemistry and Molecular Biosciences, Coopers Road, The University of Queensland St Lucia Campus, Queensland 4072, Australia. Tel. +61 7 3365 4873; fax: +61 7 3365 4699.
E-mail address: p.dodd@uq.edu.au (P.R. Dodd).

http://dx.doi.org/10.1016/j.neuint.2015.04.004
0197-0186/

the target fragment ion. A major drawback of this approach is the significant investment in development required for each peptide of interest, which currently limits assays to ~100 transitions per run (Gillet et al., 2012).

The non-targeted quantification technique SWATH™ (Sequential Window Acquisition of all THeoretical fragment-ion spectra) utilizes information-independent acquisition to scan a useful *m/z* range using wide precursor-isolation windows to collect fragment-ion spectra, at high resolution, for all analytes detected in a sample (Gillet et al., 2012). In standard SWATH acquisition, 32 precursor windows 25 Da in width are sequentially selected in the first quadrupole. In the second quadrupole, transmitted ions are fragmented and the product ions then detected in the ToF (Time of Flight) mass analyzer (Fig. 1). SWATH acquisition generates a 3D fragment-ion *m/z* intensity-retention time map for each precursor isolation window. A parallel information-dependent acquisition (IDA) experiment is used for protein identification and to generate a reference map of all the precursor and fragment ions in the sample, which permits targeted data extraction to correlate fragment-ion peaks for peptide quantification. SWATH provides quantification that is much more accurate than immunoblotting and high-throughput comprehensive data (Gillet et al., 2012), and post-acquisition data mining without upfront assay development. A major advantage is that a great number of MRM-quality assays can be performed simultaneously. SWATH has been used to quantify proteins in human plasma and cells, and to study protein interaction dynamics (Collins et al., 2013; Haverland et al., 2014). However, it has not been applied to study a subcellular fractionation proteome, including synaptosomes, from human AD autopsy tissue.

Here, we fractionated synaptosome extracts by strong cation exchange (SCX) prior to SWATH-based IDA to generate a comprehensive list of fragment ions. We compared the expression of synaptic proteins from AD-affected (hippocampus) and relatively spared (motor cortex) areas in AD and non-AD human autopsy tissue. To the best of our knowledge, this is the first study to quantify synaptosomal fractions from human autopsy tissue by SWATH. A total of 30 proteins showed greater than 1.5-fold differences in AD and non-AD comparisons.

2. Materials and methods

2.1. Tissue collection and storage

Brain tissue was obtained from the Queensland Brain Bank, School of Chemistry and Molecular Biosciences, The University of Queensland with informed written consent from the next of kin. The Queensland Brain Bank is the Brisbane node of the Australian Brain Bank Network, which is supported by the National Health and Medical Research Council. Post-mortem histopathological examination was conducted by qualified pathologists, and tissue samples were treated as per Chang et al. (2014b). The Medical Research Ethics Committee of The University of Queensland approved the study (Clearance N° 0000105).

2.2. Case selection

Clinical information including age, post-mortem interval, brain weight, and cause of death was acquired from the Queensland Brain Bank database. Pieces (0.5 g) of tissue from the pathologically affected hippocampus and the relatively spared primary motor cortex were taken from six female AD cases (71–87 y) and six female neurologically normal controls (71–91 y). This controlled for case-to-case variation in post-mortem interval and age-related factors (Chang et al., 2013); age and post-mortem interval were matched as closely

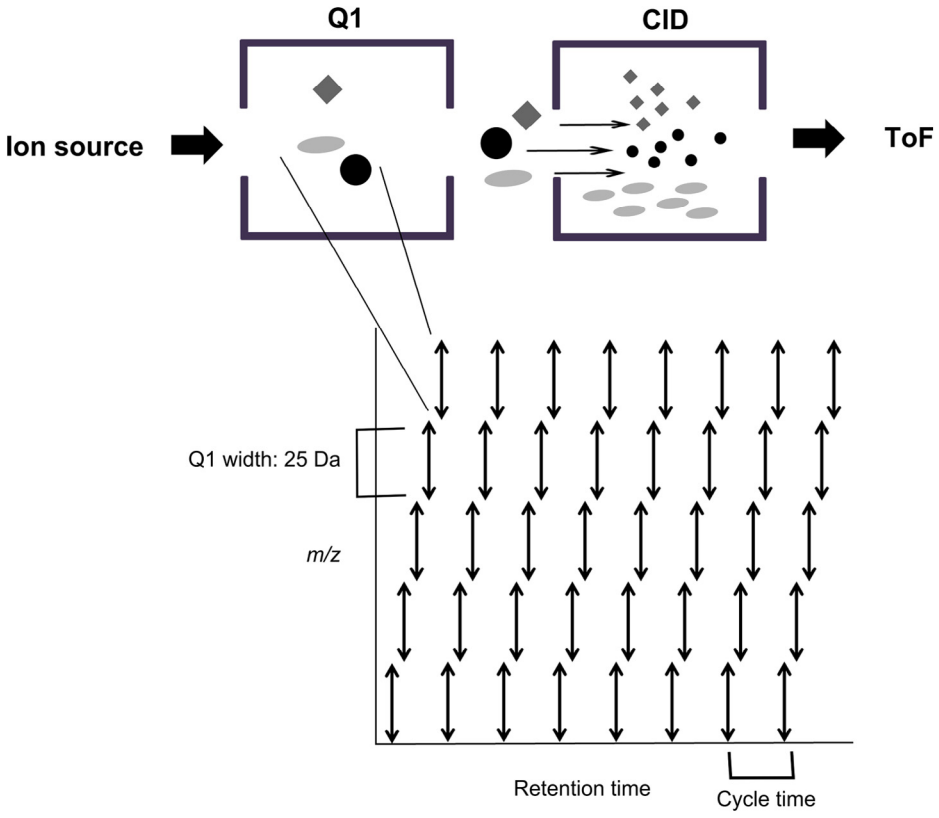

Fig. 1. Overview of SWATH acquisition. The first quadrupole (Q1) is stepped continuously with *m/z* window of 25 amu across the entire *m/z* range of interest. All fragment ions generated by collision-induced dissociation in the second quadrupole (Q2) are monitored by the ToF mass analyzer.

Table 1
Case information.

Age (y)	PMI (h)	Brain weight (g)	Cause of death
Non-AD normal controls			
69.67	23.0	1166	Hypostatic pneumonia
71.10	7.8	1204	Sudden cardiac death
75.78	48.8	1210	Pneumonia
77.57	18.0	1272	Respiratory arrest
83.65	26.0	1157	Pulmonary embolus
87.38	27.0	1398	Not determined*
AD cases			
71.33	27.0	1140	Not determined*
78.51	7.50	990	Alzheimer's disease
82.06	41.3	1100	Not determined*
84.79	35.6	1187	Dementia
89.51	19.5	1040	Not determined*
90.67	46.8	1100	Pneumonia, dementia

Note: The Cause of Death Certificate was used by the Queensland Brain Bank to ascertain the cause of death. In some instances (*), the cause of death was not recorded.

as possible between groups. All subjects were of Northern European ancestry; note that ethnicity has no significant effect on AD progression (Chang et al., 2014b). Clinical details of the cases are set out in Table 1.

2.3. Subcellular fractionation

Well-characterized synaptosomes (Dodd et al., 1981) were prepared as previously described (Chang et al., 2014a). Tissue pieces from each cortical region were homogenized in a motor-driven Teflon-glass homogenizer with 5 mL of ice-cold 0.32 M sucrose containing a phosphatase inhibitor cocktail (1 mM sodium orthovandate, 10 mM sodium pyrophosphate, 2 mM β-glycerol phosphate and 30 mM sodium fluoride). The mixture was centrifuged at 750 × *g* (J20 rotor J26-XPI centrifuge, Beckman Coulter P/L, Lane Cove, NSW, Australia) for 10 min at 4 °C. The supernatant was further centrifuged at 19 000 × *g* for 20 min at 4 °C. The pellet was re-suspended in 5 mL of 0.32 M sucrose and layered onto a density gradient consisting of 0.8 M sucrose above 1.2 M sucrose. The mixture was centrifuged at 82 500 × *g* in a swinging bucket rotor (SW41Ti, Beckman L8-60M ultracentrifuge) for 2 h at 4 °C. The synaptosomal fraction was obtained by aspirating the material at the 0.8 M–1.2 M sucrose layer interface.

2.4. Sample preparation

A 1/9 volume of 0.4% deoxycholic acid was added to the synaptosomal fraction and the mixture incubated on ice for 30 min, then incubated with 1/9 volume of 1 M trichloroacetic acid for a further 60 min. After centrifugation at 10 000 × *g* for 10 min at 4 °C, 1 mL of ice-cold 90% (v/v) acetone was added to the pellet with brief vortexing. The mixture was incubated at –20 °C overnight, then centrifuged at 10 000 × *g* for 20 min at 4 °C. The pellets were dried for 5 min, then resuspended in 25 µL of 8 M urea, 2 M thiourea in 50 mM ammonium bicarbonate. A 2D-Quant kit was used to determine protein concentration (GE Healthcare Life Sciences, Rydalmere, NSW, Australia). An equal amount of each sample was pooled to generate 30 µg of synaptosomal fraction. An aliquot (5 µg) of each samples and a pooled sample (30 µg) were brought to 5 mM in dithiothreitol and incubated for 120 min at room temperature. Iodoacetamide was added to a final concentration to 25 mM and the mixture incubated for 30 min in the dark. Dithiothreitol was added to a final concentration of 10 mM to quench excess iodoacetamide. Samples were diluted to 2 M urea with 50 mM ammonium bicarbonate. Trypsin was added at 1:100 (enzyme:protein) ratio, and the mixture incubated for 6 h at 37 °C. An equal amount of trypsin was added, followed by overnight incubation at 37 °C. Trypsin-digested peptides were purified and concentrated using a ZipTipC_{18} (10 µL tip with 0.6 µL resin bed, Millipore, Billerica, MA, USA) according to the manufacturer's instructions. A pooled sample was subjected to SCX fractionation prior to LC-MS/MS.

2.5. Strong cation exchange fractionation

The samples were dissolved in buffer A (0.5% acetic acid, 2% acetonitrile), and fractionated by SCX chromatography using an Agilent 1100 series LC system (Agilent Technologies, Mulgrave, Vic, Australia) equipped with a ZORBAX BioSCX-Series II column (Agilent Technologies, 50 mm × 2.1 mm, 3.5 µm). The peptides were eluted over 32 min at 0.1 mL/min with the following linear gradients: 0% buffer B (0.5% acetic acid, 2% acetonitrile, 250 mM ammonium acetate) for 3 min, 0–15% buffer B for 2 min, 15–50% buffer B for 17 min, 50–80% buffer B for 3 min, 80% buffer B for 5 min, and 80–0% buffer B for 2 min. One-minute samples (100 µL) were collected for 37 min; eluate samples ##1–12 were combined to give Fraction 1, ##13–14 Fraction 2, #15 Fraction 3, #16 Fraction 4, #17 Fraction 5, #18 Fraction 6, ##19–20 Fraction 7, and 21–37 Fraction 8. Fractions were vacuum concentrated followed by ZipTip$_{18}$ desalting. Each was processed separately on a Triple-ToF 5600 mass spectrometer for IDA analysis.

2.6. HPLC-TripleToF 5600 mass spectrometer

Samples were analyzed using a Shimadzu Prominence nanoLC-MS/MS connected to a Triple-ToF 5600 mass spectrometer (AB SCIEX, Framingham, MA, USA). Mobile phases A_T and B_T were 1% acetonitrile/0.1% formic acid and 80% acetonitrile/0.1% formic acid respectively. SCX-separated fractions 1–8 (~1 µg) and unfractionated samples (1 µg) were loaded onto the autosampler maintained at 12 °C, then trapped in a 150 µm × 150 mm, 5 µm C_{18} column and desalted for 3 min with 100% mobile phase A_T at a flow rate of 30 µL/min. Injection volume was 10 µL for standard IDA experiments and 15 µL for SWATH experiments; sample mass was 1 µg in each instance. Chromatographic separations were performed using a Vydac Everest C_{18} column (150 µm ID × 150 mm, 300A, 5 µm particle size; Mandel Scientific, Guelph, ON, Canada) with following linear gradient: 10% buffer B_T from 0–3.01 min, 10–60% buffer B_T from 3.01–48 min, 60–97% buffer B_T from 48–56 min, 97% buffer B_T from 56–61 min, 97–10% buffer B_T from 61–63 min, and 10% buffer B_T from 63–70 min, at a flow rate of 1 µL/min. Eluted peptides were detected by TripleToF 5600 MS (AB SCIEX) coupled with a Nanospray III ion source in positive ion mode using PicoTip Emitter SilicaTips (12 cm, 10 µm diameter, uncoated; New Objective, Woburn, MA, USA). The following MS conditions were used: declustering potential of 80 V, curtain gas of 30 psi, gas #1 of 10 psi and interface heater temperature of 150 °C.

2.7. IDA experiment

For ToF mass spectrometry (MS) scans, ions with *m/z* values between 350 and 1800 were analyzed with an accumulation time of 0.5 s. For MS/MS, ions between *m/z* 40 and 1800 were acquired in high-sensitivity mode with accumulation time of 0.05 s, and up to 20 product ions with 2 + to 5 + charge-state were collected if they exceeded an intensity threshold of 100 cps. Total cycle time was 1.55 s. Four time bins were summed for each scan, with 1.059 ms pauses between mass ranges. A sweeping collision energy of 40 ± 15 V was applied for collision-induced dissociation. The MS was auto-calibrated using a tryptic digest of 5 fmol of β–galactosidase by using peptides at *m/z* 534.2489, 542.2645, 550.2802, 671.3379, 714.8469 and 729.3652, and fragment ions of the peptide at *m/z*

729.3652 for MS/MS mode. Each of SCX fractions 1–8 was run separately and the analysis was repeated three times.

2.8. SWATH experiment

For SWATH–based experiments, the mass spectrometer was operated in a looped product ion mode. For the MS1 scan, the mass range 350–1800 Da was analyzed with an accumulation time of 50 ms. A set of 34 overlapping windows was then constructed with an isolation width of 26 Da (contains 1 Da for the window overlap; Gillet et al., 2012) to cover the mass range 400–1250 Da (cycle time 3.33 s). The collision energy was independently determined using Analyst software (AB SCIEX) for each window based on the calculation for a 2+ ion centered upon the window with a collision energy spread of 15 V, linearly across the accumulation time (95.1 ms). Fragment-ion scans were in high-sensitivity mode.

2.9. IDA data analysis

ProteinPilot software v. 4.5 (AB SCIEX) was used to process IDA data. IDA files from triplicate runs of Fractions 1–8 were combined for the search. False discovery rate analysis was done with tools integrated in the software. The thorough ID search setting was selected with the following criteria: identification; cysteine alkylation, iodoacetamide; digestion, trypsin; fixed modification, carbamidomethylation; variable modification, oxidation of methionine. The detected protein *P*-value threshold was set to 0.05.

2.10. Data processing and statistical analysis

ProteinPilot results were exported to PeakView software (AB SCIEX) for identification, quantification and alignment of spectral peaks. Shared peptides and peptides with confidence level below 99% were excluded. The number of peptides was set to 10 and transitions to 6. An ion library was created in PeakView for statistical analysis using MSstats. MSstats is R-based statistical software which (1) transforms and normalizes the peak intensities, (2) automatically detects the experimental design from the data, and (3) fits an appropriate linear mixed model. The peak areas were normalized to equalize median endogenous intensities across runs. Two comparisons were made: AD hippocampus *vs.* AD motor cortex and non-AD hippocampus *vs.* AD motor cortex. Proteins that showed greater than ± 1.2-fold difference with adjusted *P*-value of < 0.05 were subjected to further analysis, where each spectral peak was manually inspected in PeakView software to confirm the identity of the selected peak. The retention times of selected peptides from SWATH acquisition were also crosschecked with the reference map. MS/MS spectra were carefully checked to confirm the peptide sequence by matching it to the theoretical fragment ions; peptides that could not be confirmed were removed from the ion library. Peptides with spectral peaks with intensity lower than 800 were excluded. Proteins with less than two peptides were excluded. Peptides containing potential PTM sites (according to Uniprot) were noted. The updated ion library was subjected to further statistical analysis in MSstats. Proteins that showed greater than ± 1.3-fold difference with adjusted *P*-value of < 0.05 were considered significant. A list of all the transitions used can be found in Supplementary Table S1.

2.11. Pathway analysis

Differentially expressed proteins were subjected to IPA software (Ingenuity Systems, Redwood City, CA, USA) to evaluate the most relevant interaction networks and to identify other proteins associated with those networks. Protein accession numbers were imported into IPA for analysis. IPA generates protein interaction networks in silico based on protein–protein interactions and associations mined from the peer-reviewed literature. Proteins were represented as nodes and biological associations between nodes were linked. Different node shapes were used to represent functional variants of proteins (Fig. 3).

3. Results

3.1. Reference map

To generate spectral libraries for a reference map of the synaptosomal fraction from human brain, a pooled sample from AD and non-AD hippocampus and motor cortex was analyzed. The pooled sample was divided into 8 fractions by SCX; each fraction was analyzed separately, in triplicate, using SWATH-based IDA LC-MS/MS. Results were analyzed together using ProteinPilot Software, which uses the Paragon algorithm for protein identification. The Proteomics System Performance Evaluation Pipeline determined the independent false discovery rate of the Paragon data. A total of 2077 different proteins were identified (Supplementary Table S2) that had a critical local false discovery rate < 5%. This is ~1800 more identifications than SWATH-based IDA analysis without prior SCX-fractionation (Supplementary Table S3). For each peptide, precursor ion sequence, mass, charge, and chromatographic retention time, and fragment ion mass, charge, and relative intensities were collected.

3.2. Differentially expressed synaptic proteins

In total, 68 proteins showed significant expression differences between AD or non-AD hippocampus when compared with motor cortex, and > 1.5-fold differences in AD *vs.* non-AD comparisons, i.e. [the difference between AD hippocampus and AD motor cortex] *vs.* [the difference between normal control hippocampus and normal control motor cortex]. These comparisons were made because human subjects are highly variable in age, gender, medication, and cause of death. These potential confounds could affect the synaptic proteome. To counter these factors, the severely affected hippocampus within each group was compared with the relatively spared motor cortex. Transitions representing each peptide that belonged to a given protein were manually inspected to exclude (i) noise-like signals, (ii) peptides with MS/MS spectra that could not confidently be matched to theoretical spectra, (iii) peptides with known PTM sites, and (iv) peptides that had different retention times from those in the spectral library derived from IDA analysis. The same statistical test was conducted again with these peptides excluded, and it was found that 30 unique proteins showed >1.5-fold differences in AD *vs.* non-AD comparisons (Table 2). Rabphilin-3A expression showed a –2.6-fold difference (<0.001) in AD hippocampus than in AD motor cortex and +1.9-fold difference (<0.001) in non-AD hippocampus when compared with non-AD motor cortex. Neurofilament proteins showed significantly lower expression in AD hippocampus and non-AD hippocampus when compared with AD motor cortex and non-AD motor cortex respectively, but the extent of difference was greater in the within-AD comparisons. The expression levels of all the septin proteins subjected to pathway analysis (septin 2, 5, 7, 8, 9 and 11) were significantly lower in AD hippocampus than in AD motor cortex, whereas expression levels did not differ significantly for septin 2, 8, 9 or 11 in the hippocampus-motor cortex comparison in non-AD tissues. The extent of difference for the within-AD comparison was greater for all the septins except for septin 5, which was notably larger in normal controls. Transitions for the 30 proteins are presented in Supplementary Table S1.

3.3. Pathway analysis

Proteins exhibiting expression differences were further analyzed by core Ingenuity Pathway Analysis (IPA) to gain insight into

Table 2
Proteins identified with significant expression differences in hippocampus compared with motor cortex in AD and non-AD patients.

Acc #	Gene name	Name	AD		Non-AD	
			Fold difference	*P*-value	Fold difference	*P*-value
Q16352	INA	α-internexin*	−2.3	<0.001	−1.4	<0.001
Q02246	CNTN2	Contactin 2*	−2.1	<0.001	−1.2	0.360
P13611	VCAN	Versican core protein	−2.0	<0.001	−1.4	<0.001
Q9NZN3	EHD3	EH domain-containing protein 3*	−1.2	<0.001	1.1	0.036
P12036	NEFH	Neurofilament heavy polypeptide	−3.0	<0.001	−1.7	<0.001
P07196	NELE	Neurofilament light polypeptide*	−2.3	<0.001	−1.3	<0.001
P07197	NEFM	Neurofilament medium polypeptide*	−2.1	<0.001	−1.2	<0.001
Q15365	PCBP1	Poly C-binding protein 1	−1.4	<0.001	−1.1	0.131
Q9Y3C6	PPIL1	Peptidyl-prolyl cis-trans isomerase-like 1	1.6	0.002	−1.1	0.739
P32119	PRDX2	Peroxiredoxin-2, isoform 1*	−1.4	<0.001	−1.1	<0.001
P28072	PSMB6	Proteasome subunit β type 6	1.7	0.001	−1.1	0.861
P84095	RHOG	RhoG	−1.6	<0.001	1.1	0.713
Q15019	SEPT2	Septin 2	−1.2	<0.001	−1.1	0.087
Q99719	SEPT5	Septin 5	−0.7	<0.001	−1.2	<0.001
Q16181	SEPT7	Septin 7	−1.6	<0.001	−1.2	<0.001
Q92599	SEPT8	Septin 8*	−1.3	<0.001	−1.1	0.271
Q9UHD8	SEPT9	Septin 9	−1.3	<0.001	−1.1	0.619
Q9NVA2	SEPT11	Septin 11*	−1.4	<0.001	−1.2	0.001
Q9C0H9	SRCIN1	SRC kinase signaling inhibitor 1	1.6	<0.001	0.0	0.856
Q92777	SYN2	Synapsin 2*	1.2	<0.001	1.5	<0.001
P68366	TUBA4A	Tubulin α-4A chain	−1.4	<0.001	0.0	0.912
P04350	TUBB4A	Tubulin β-4A chain	−1.3	<0.001	1.1	0.160
Q99726	SLC30A3	Zinc transporter 3*	−1.7	<0.001	1.2	0.511
P60520	GABARAPL2	γ-aminobutyric acid receptor-associated protein-like 2	−1.2	0.144	−1.4	<0.001
Q13423	NNT	NADP transhydrogenase, mitochondrial	0.0	0.665	1.4	<0.001
Q99536	VAT1	Vesicle amine transport 1	0.0	0.601	1.2	<0.001
Q9Y2I8	WDR37	WD repeat-containing protein 37	−1.2	0.040	−1.1	0.687
O94811	TPPP	Tubulin polymerization-promoting protein*	−1.6	<0.001	−1.3	<0.001
Q9Y2J0	RPH3A	Rabphilin-3A*	−2.6	<0.001	1.9	<0.001
P36957	DLST	2-oxoglutarate dehydrogenase complex component E2, mitochondrial*	−1.5	<0.001	−1.3	<0.001

Note: Each protein is listed with SwissProt accession number, sequence coverage, $\log_2$ fold change (significant if value is greater than ± 0.3), and *P* value (generated by MSstats statistical software; significant differences in italics). *, has been implicated in AD in previous studies.

the most relevant cellular functions and networks altered in AD, and to identify other closely associated proteins. The most perturbed molecular and cellular functions in AD hippocampus were cellular assembly and organization, cellular function and maintenance, cell-to-cell signaling and interaction, cell morphology, and cellular development. The top disease/disorder was neurological disease, and the top physiological system development and function was nervous system development and function. Core analysis revealed RhoA signaling (septins 2, 5, 7, 8, 9 and 11 are associated) to be the top canonical pathway, followed by signaling by Rho family GTPases (RhoG and septins 2, 5, 7, 8, 9 and 11 are associated; Fig. 2). Network analysis showed that differentially expressed proteins were related to cellular assembly and organization, cellular function and maintenance, and nervous system development and function. This top-ranked network was visualized in IPA, which revealed other closely associated proteins (Fig. 3): ubiquitin C, serine/arginine repetitive matrix 2, sirtuin 7, tubulin β-3 chain, tubulin β-4B chain, septin 9, and presenilin 1.

4. Discussion

We used SWATH-based mass spectrometry to compare the expression of synaptosomal proteins from AD and non-AD hippocampus and motor cortex. The prevalence of Alzheimer's disease is higher in females than in males (Baum, 2005), for reasons that are unclear: there is no evidence for any *pathological* difference between the sexes. Human subjects vary widely in age, gender, post-mortem interval, medication, cause of death and other factors. Hence, we limited the study to females to reduce complexity. The sensitivity of SWATH is such that if there is indeed a sex difference

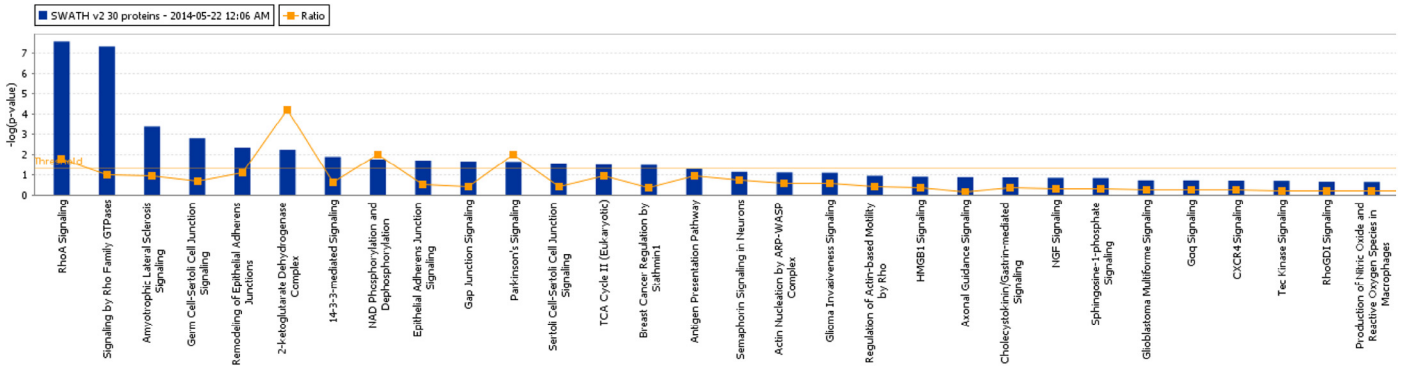

Fig. 2. Top canonical pathways from IPA core analysis.

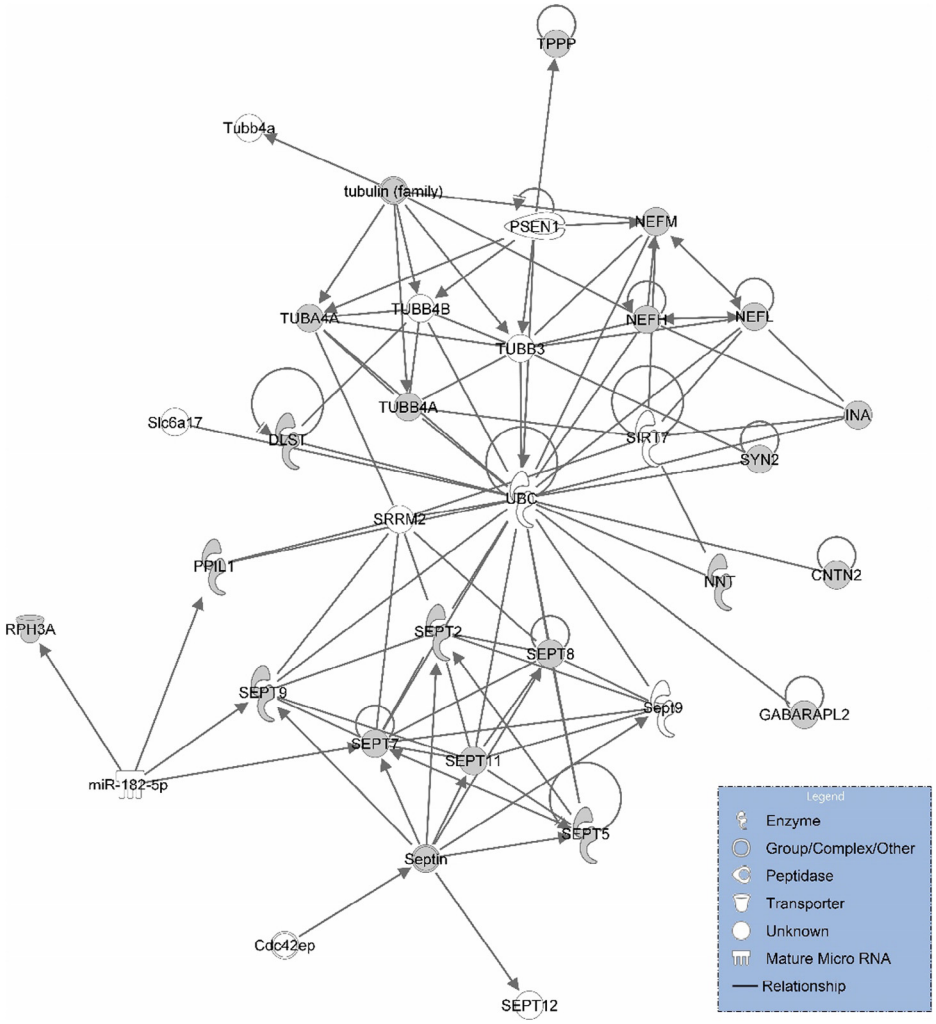

Fig. 3. Pathway analysis. Identified proteins are shaded. TPPP, tubulin polymerization-promoting protein; TUBB4A, tubulin β-4A class IVa; PSEN1, presenilin 1; NEFM, neurofilament medium polypeptide; TUBA4A, tubulin α-4A chain; TUBB4B, tubulin β-4B chain; TUBB3, tubulin β-3 chain; NEFH, neurofilament heavy polypeptide; NEFL, neurofilament light polypeptide; SLC6A17, solute carrier family 6 member 17; DLST, dihydrolipoyllysine-residue succinyltransferase component of 2-oxoglutarate dehydrogenase complex, mitochondrial; TUBB4A, tubulin β-4A chain; UBC, ubiquitin C; SIRT7, sirtuin 7; SYN2, synapsin 2; INA, α-internexin; SRRM2, serine/arginine repetitive matrix 2; PPIL1, peptidylprolyl isomerase-like 1; NNT, nicotinamide nucleotide transhydrogenase; CNTN2, contactin 2; RPH3A, rabphilin; SEPT2, septin 2; SEPT5, septin 5; SEPT7, septin 7; SEPT8, septin 8; SEPT9, septin 9; SEPT11, septin 11; SEPT12, septin 12; GABARAPL2, $GABA_A$ receptor-associated protein-like 2.

in pathology that is reflected in protein expression, this approach is most likely to be able to detect it, and thus we would need to have included at least twice as many subjects to undertake the necessary analysis. This was difficult both on cost grounds and because we first needed to establish the veracity of the methodology. The data presented will underpin a future SWATH-SCX study comparing males and females, which should provide new insights into this issue. Gillet et al. (2012) showed that SWATH-based protein quantification provides MRM-like quality that is highly consistent and accurate. The present study is the first to use SCX-fractionation prior to SWATH-based IDA to generate a comprehensive reference map of a proteome. We partitioned sample complexity by dividing the samples into eight different fractions, each of which was analyzed separately. Spectral data from each fraction were combined to generate a reference map of 2077 unique proteins. Without prior SCX-fractionation, around 536 proteins were identified using SWATH-based IDA analysis. This showed that reducing sample complexity greatly increases the likelihood of identifying less-abundant proteins. These may have been undetected due to the matrix effect, in which ionization efficiency is altered because of co-eluting substances.

SWATH data processing software is in early stages of development. We found that the software often selected a peak that does not belong to the target peptide: (i) its retention time differed greatly when crosschecked with the reference map; and/or (ii) the peptide sequence could not be confirmed when MS/MS spectra were matched to the theoretical fragment ions. For example, PeakView software suggested that peptide NLLHQDAVDLFT (3+) from synaptojanin-2-binding protein was eluted at 16.9 min (Fig. 4A); however, the MS/MS spectrum at 16.9 min did not relate to the target peptide sequence. Rather, the peptide sequence could be confirmed at 17.6 min (Figs 4C and 4D). Unfortunately, the user cannot de-select the spectral peak that the software chooses and re-select the correct one. In addition, peak identification cannot depend solely on the accuracy of retention time (Fig. 5). The observed retention time of peptide ESIDLVLDR from tubulin α-8 chain was 20.9 min, whereas the reference map stated 15.9 min. When the MS/MS spectra of the peptide were checked, the spectral peak truly represented the target (Figs 5B and 5C). Only peptides manually confirmed as correct were quantified.

Thirty unique proteins showed (i) significant differences in expression between AD hippocampus and AD motor cortex and/or

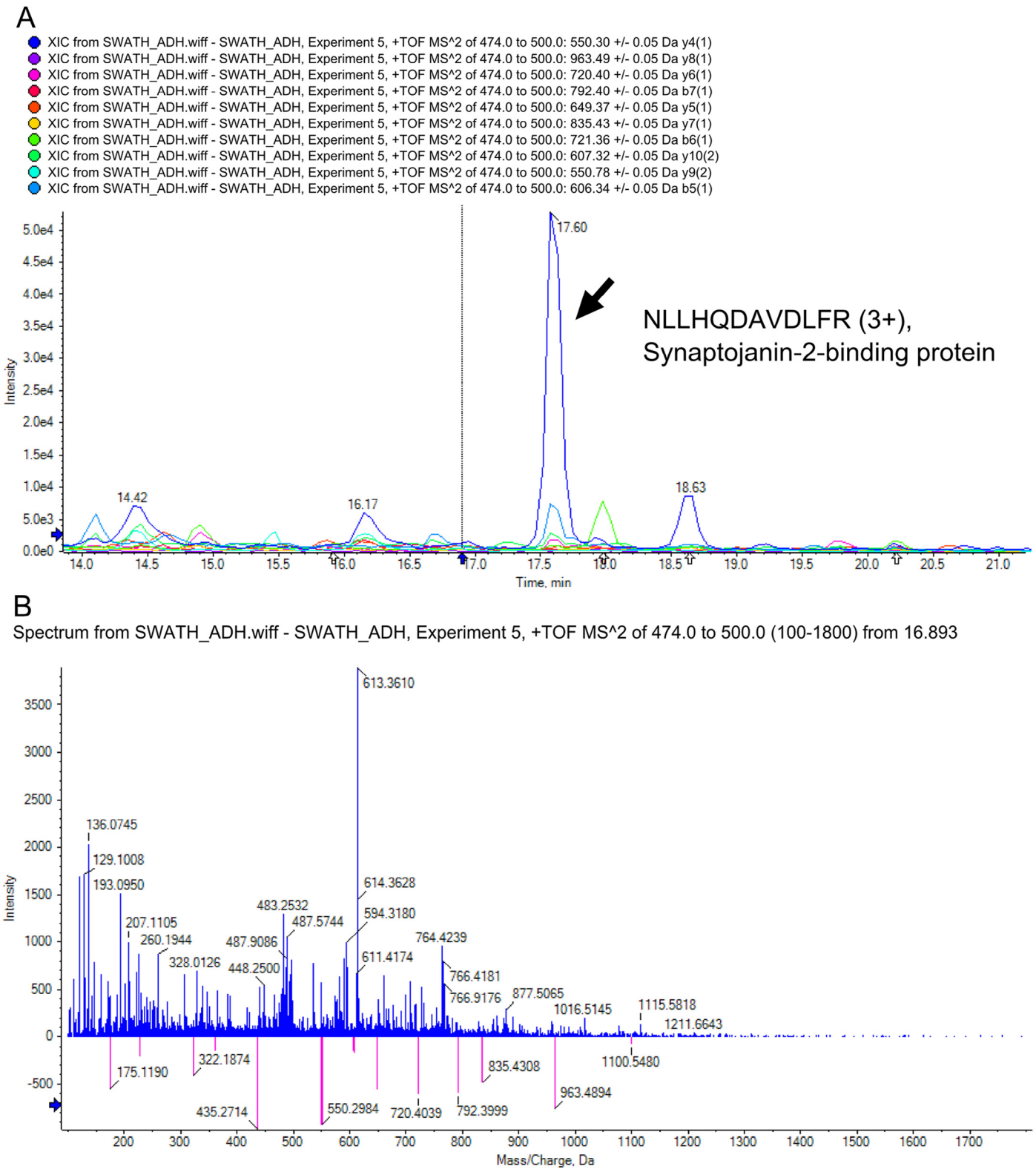

Fig. 4. Triply charged peptide NLLHQDAVDLFR from synaptojanin-2-binding protein. (A) Spectral peaks detected at SWATH window 474.0 to 500.0 *m/z* between 13.8 and 21.2 min. Blue arrow points to spectral peaks that Peakview software selected. Black arrow points to spectral peaks that actually belong to the target peptide. (B) MS/MS spectrum at 16.9 min. Blue represents the spectrum from the SWATH data and the matching peaks are displayed in pink. (C) Peptide fragments. (D) MS/MS spectrum at 17.6 min. Peaks that could be identified at theoretical fragment ion *m/z* value are marked with black rectangular boxes.

non-AD hippocampus and non-AD motor cortex, and (ii) > 1.5-fold differences in AD *vs.* non-AD comparisons. Of these, 13 proteins have previously been implicated in AD pathology, and 17 are novel (Table 2). This study alone cannot identify unequivocally the mechanisms that underlie synaptic dysfunction in AD: but altered expression could be detrimental to synaptic function. Differentially expressed proteins were classified into functional groups.

C

Peptide fragments

	Symbol	Res. Mass	# (N)	b	b - 17	b - 18	y	y - 17	y - 18	# (C)
	N	114.04293	1	115.05020	98.02365	97.03964	1440.75939	1423.73284	1422.74883	12
	L	113.08406	2	228.13427	211.10772	210.12370	1326.71646	1309.68991	1308.70590	11
	L	113.08406	3	341.21833	324.19178	323.20777	1213.63240	1196.60585	1195.62183	10
	H	137.05891	4	478.27724	461.25069	460.26668	1100.54833	1083.52178	1082.53777	9
	Q	128.05858	5	606.33582	589.30927	588.32526	963.48942	946.46287	945.47886	8
	D	115.02694	6	721.36276	704.33622	703.35220	835.43084	818.40430	817.42028	7
	A	71.03711	7	792.39988	775.37333	774.38931	720.40390	703.37735	702.39334	6
	V	99.06841	8	891.46829	874.44174	873.45773	649.36679	632.34024	631.35622	5
	D	115.02694	9	1006.49524	989.46869	988.48467	550.29837	533.27182	532.28781	4
▶	L	113.08406	10	1119.57930	1102.55275	1101.56874	435.27143	418.24488	417.26087	3
	F	147.06841	11	1266.64771	1249.62116	1248.63715	322.18737	305.16082	304.17680	2
	R	156.10111	12	1422.74883	1405.72228	1404.73826	175.11895	158.09240	157.10839	1

D

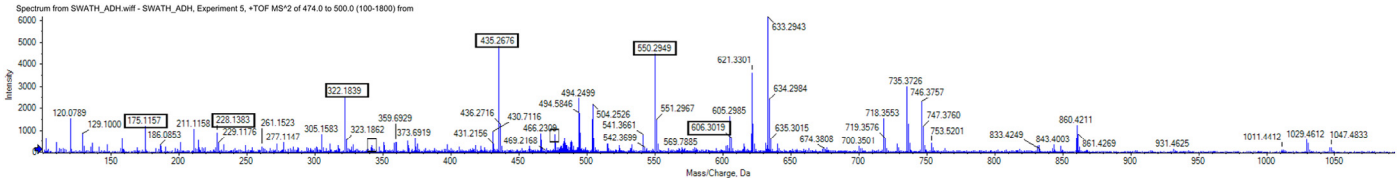

Fig. 4. (*continued*)

4.1. Structural proteins

The expression of the structural proteins that included the septins, adhesion molecules, neurofilaments, tubulin, and tubulin polymerization-promoting protein differed between AD and non-AD hippocampus. Altered expression of structural proteins might impair structural integrity and axonal transport mechanisms, and lead to synaptic atrophy.

We identified septins 2, 3, 4, 5, 6, 7, 8, 9 and 11 in the synaptosome fraction, and we were able to quantify all. For septin 3, proteotypic peptides detected by IDA belonged to isoforms 1 and 2, but not 3. Hence, the difference did not represent global septin 3 expression, nor was it isoform-specific. As a result, septin 3 was excluded from further analysis. Six proteotypic peptides (with > 99% confidence score) were used to identify septin 5. Of these, four (ELKESAPFAVIGSNTVVEAK, ESAPFAVIGSNTVVEAK, STLVHSLFLTDLYK and STLVHSLFLTDLYKDR) are in all isoforms, and two (MESPIPILPLPTPDAETEKLIR and MESPIPILPLPTPDAETEK) are specific to isoform 1. The latter two sequences differ by only three amino acids (LIR). Although transitions from two peptides were considered acceptable, we felt it would be unreliable to depend on two peptides that shared the long peptide sequence MESPIPILPLPTPDAETEK. One proteotypic peptide was detected for septin 8 isoform 1. Because using transitions from a single peptide is not reliable for quantification, septin 8 isoform 1 (SLSLGGHVGFDSLPDQLVSK) could not be confidently analyzed.

Septin 4 and septin 6 did not show significant expression differences, while all other septins examined showed significantly lower expression in AD hippocampus than in AD motor cortex. Septins 8 and 11 expression differences were found in our previous AD study using 2D gel electrophoresis (Chang et al., 2013). Septin 8 was identified from two protein spots in AD hippocampus, where one showed significantly higher expression and one showed no change. When temporal cortex was compared with occipital cortex, septin 11 expression was higher in non-AD brain but no significant difference was seen in AD brain. The 2D gel results could reflect a difference in expression of the isoform and/or its post-translationaly modified forms, which will be invaluable information if the nature of the modification can be determined. SWATH results reported here are global differences, not isoform switching or modification. Previous studies have shown that lower septin 2, 5, 7 (Tada et al., 2007) and 11 (Li et al., 2009) expression disturbs the cytoarchitecture of spines and dendritic arborization. Septin 5 may be involved in exocytosis by regulating SNARE function (Beites et al., 2005) and septin 11 plays a role in γ-aminobutyric acidergic synaptic connectivity (Li et al., 2009). Since septins are functionally related to vesicle trafficking and the cytoskeleton, they may be essential for neurotransmitter release and the regulation of axon development. Thus, down-regulation of septins could alter neurotransmission and synaptic structure in AD hippocampus.

Contactin 2 is a cell adhesion molecule highly expressed at the axon that regulates axon guidance and neurite outgrowth (Baeriswyl and Stoeckli, 2008). In knockout mice, contactin 2 is essential for regulating normal learning and memory (Savvaki et al., 2008). We found significantly lower expression of contactin 2 in AD hippocampus and non-AD hippocampus than in AD motor cortex and non-AD motor cortex respectively; the difference was more than 3-fold in AD hippocampus. Gautam et al. (2014) reported that contactin 2 expression was lower in AD temporal cortex than in an age-matched control sample. Thus, contactin 2 may be down-regulated in whole tissue as well as within synapses in AD-affected areas. This may cause structural damage by perturbed cellular adhesion.

Decreased expression of α-internexin (INA) has been found in an AD transgenic mouse model (Takano et al., 2013), and increased expression in the postsynaptic density in human AD autopsy cortex (Zhou et al., 2013). We found significantly lower expression of INA in synaptosomal fractions from AD and non-AD hippocampi compared with AD and non-AD motor cortices respectively (Fig. S1); however, the difference was more than two-fold in AD hippocampus. A similar decrease was reported in neurofilament light polypeptide (NFL) and neurofilament medium polypeptide (NFM) transcript in AD brain from Northern blots (Kittur et al., 1994).

A

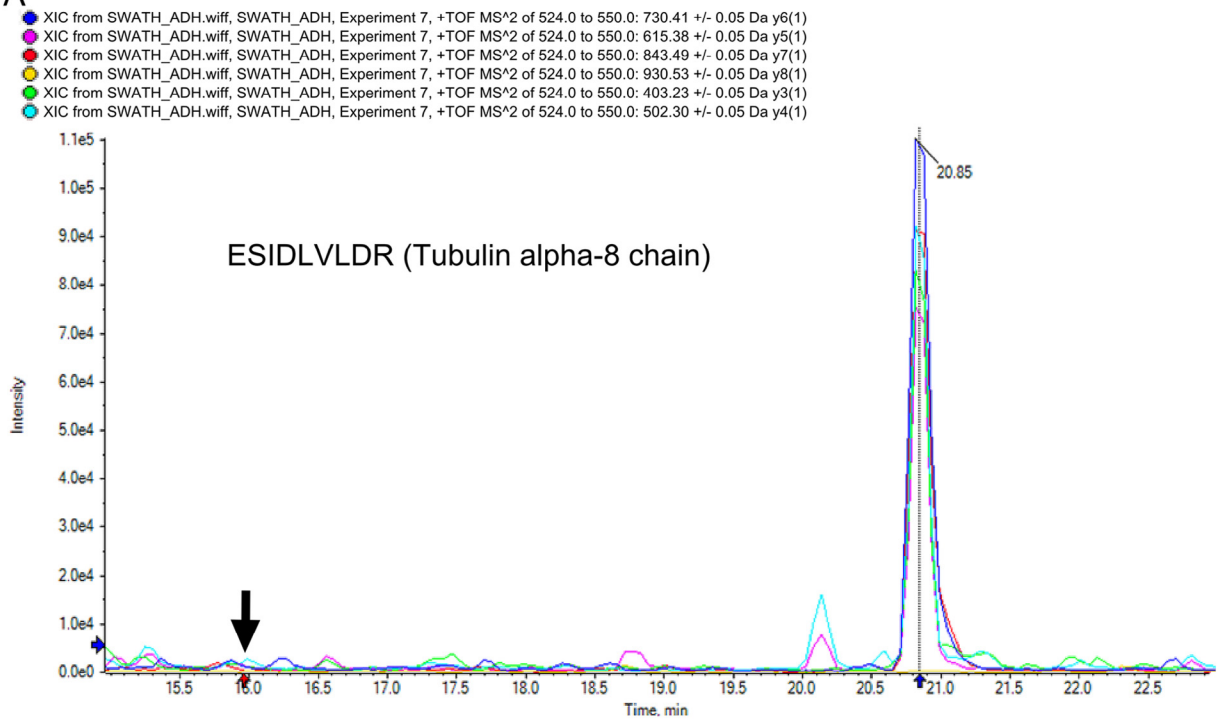

B

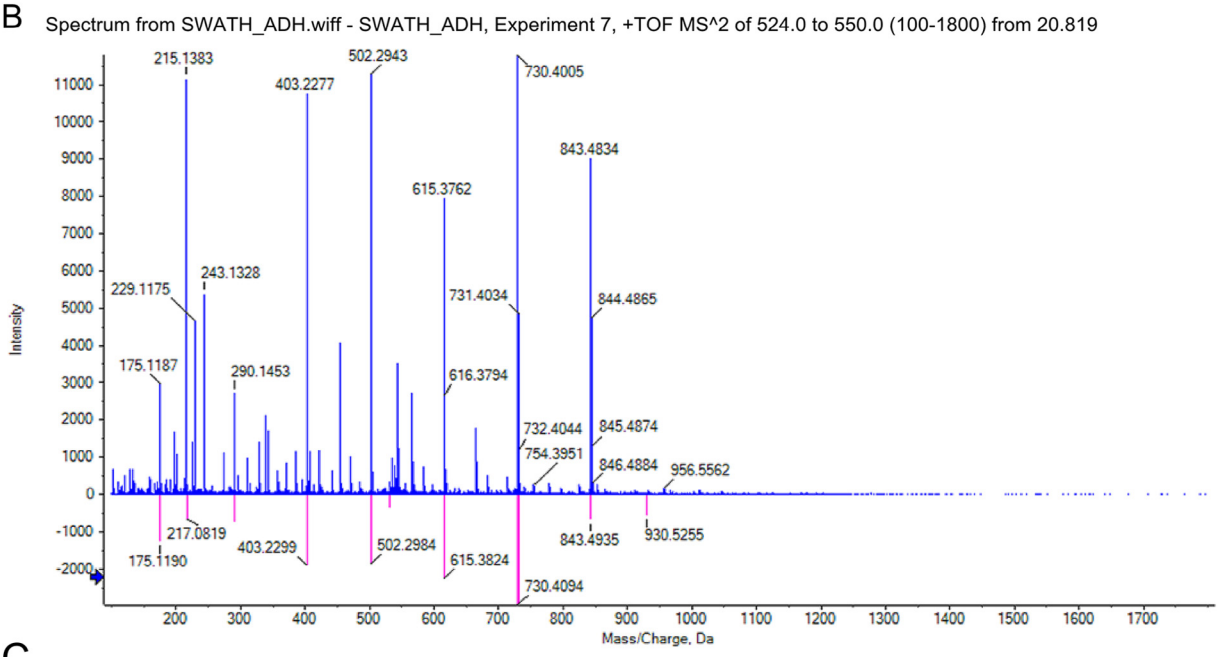

C Peptide fragments

	Symbol	Res. Mass	# (N)	b	b - 17	b - 18	y	y - 17	y - 18	# (C)
▶	E	129.04259	1	130.04987	113.02332	112.03930	1059.56807	1042.54152	1041.55750	9
	S	87.03203	2	217.08190	200.05535	199.07133	930.52547	913.49892	912.51491	8
	I	113.08406	3	330.16596	313.13941	312.15540	843.49344	826.46690	825.48288	7
	D	115.02694	4	445.19291	428.16636	427.18234	730.40938	713.38283	712.39882	6
	L	113.08406	5	558.27697	541.25042	540.26640	615.38244	598.35589	597.37187	5
	V	99.06841	6	657.34538	640.31883	639.33482	502.29837	485.27182	484.28781	4
	L	113.08406	7	770.42945	753.40290	752.41888	403.22996	386.20341	385.21939	3
	D	115.02694	8	885.45639	868.42984	867.44583	290.14590	273.11935	272.13533	2
	R	156.10111	9	1041.55750	1024.53095	1023.54694	175.11895	158.09240	157.10839	1

Fig. 5. Peptide ESIDLVLDR from tubulin α-8 chain. (A) Spectral peaks detected in SWATH window 524.0 to 550.0 *m/z* between 15.0 and 23.0 min. Blue arrow points to spectral peaks eluting at 20.9 min, which the Peakview software selected. Black arrow points to peaks eluting at 15.9 min, which the reference map suggests. (B) MS/MS spectrum at 20.9 min. Blue represents the spectrum from the SWATH data and the matching peaks are displayed in pink. (C) Peptide fragments. Peaks identified at theoretical fragment ion *m/z* value are marked with a black rectangular box.

This suggests that the loss of INA expression in pre-synapses is severe in AD brain. Significantly lower levels of these structural proteins in AD hippocampal synapses may alter synaptic morphology and function.

Three proteins associated with microtubules were differentially expressed in AD hippocampus: tubulin α-4A chain, tubulin β-4A chain, and tubulin polymerization-promoting protein. We previously reported lower expression of tubulin polymerization-promoting protein in AD temporal cortex (Chang et al., 2013). Here, we show that its expression is significantly lower in AD hippocampus. Levels of tubulin α-4A chain and tubulin β-4A chain were also lower in AD hippocampus. This is the first report of reduced expression of these two proteins in AD hippocampal synapses. Altered expression of these microtubule-associated proteins may affect axonal transport mechanism and synaptic degeneration in AD hippocampus.

4.2. Signaling

We found poly C-binding protein 1 in the synaptosomal fraction from human brain. It is difficult to predict the role of this multifunctional protein at the synapses; however, down-regulation in the synaptosomal fraction of AD hippocampus suggests a possible disruption of gene regulation, including that of the μ-opioid receptor (Rivera-Gines et al., 2006). The opioid system is involved in cognitive and memory function, and is affected in AD brain, which shows significantly reduced numbers of μ-opioid receptors (Mathieu-Kia et al., 2001). Hence, down-regulation of poly C-binding protein 1 may disrupt the opioid system and underpin cognitive decline in AD brain.

Another protein involved in signal transduction is EH domain-containing protein 3 (EHD3). Amyloid β secretion is significantly reduced in hippocampal neurons in EHD3 knockout mice (Buggia-Prévot et al., 2013). Our previous work using 2D gels showed significant down-regulation of a protein spot representing EHD3 (Chang et al., 2013). Down-regulation of this protein may be a protective mechanism deployed by AD hippocampus to reduce amyloid β toxicity.

Versican is an extracellular matrix protein with four isoforms, V_0, V_1, V_2 and V_3, each with different functions. Peptides used to quantify versican protein were not isoform-specific, but rather, represented global expression. It may be that versican protein down-regulation reflects that of isoform V_2, as it is the dominant isoform in mature brain (Schmalfeldt et al., 1998). Isoform V_2 is involved in glutamatergic synaptic transmission and the inhibition of neurite outgrowth by organizing the extracellular matrix assembly (Dours-Zimmermann et al., 2009). Versican protein down-regulation may alter the regulation of synaptic transmission and structure, both of which are observed in AD hippocampus.

The expression of RhoG protein was significantly lower in AD hippocampus than in AD motor cortex, while there was no significant difference between non-AD hippocampus and non-AD motor cortex. Lower expression of RhoG may disturb Rho signaling at AD hippocampal synapses, and lead to structural and functional dysfunction.

Src kinase signaling inhibitor 1 (SRCIN1) inhibits Src activity and downstream signaling. SRCIN1 expression was significantly lower in AD hippocampal synapses than in those from control areas, which could lead to over-activation of glutamate-NMDA receptors. This might promote excitotoxicity, a commonly posited feature of AD brain. SRCIN1 regulates exocytosis by acting as a linker protein connecting SNAP-25 to the actin cytoskeleton (Chin et al., 2000). SRCIN1 interacts with synaptophysin, a presynaptic vesicle membrane protein (Ito et al., 2008). These studies together suggest a possible role for SRCIN1 in synaptic dysfunction as a consequence of excitotoxicity and disturbed neurotransmitter release.

Another protein involved in vesicular exocytosis, rabphilin 3A (Deak et al., 2006), was also lower in AD hippocampus than in AD motor cortex. The expression of this protein is significantly attenuated in post-mortem AD neocortex (Tan et al., 2014), supporting the hypothesis that neurotransmitter release is disturbed in AD.

4.3. Autophagy

The γ- aminobutyric acid type A receptor-associated protein-like 2 mediates the autophagy of damaged mitochondria. It is not clear whether overactive, pathologic autophagy or insufficient protective autophagy promotes ageing. We found significantly lower expression of this protein in non-AD hippocampus than in non-AD motor cortex, and no significant regional differences in AD tissues. Our finding supports the hypothesis that pathologic autophagy damages synapses in AD.

4.4. Oxidative stress

The levels of NADP transhydrogenase and peroxiredoxin-2 isoform 1 were significantly lower in AD hippocampus synaptosomes than in those from AD motor cortex, but the equivalent comparison was not significant in non-AD tissues. In contrast, peroxiredoxin-2 expression is reportedly increased in whole-tissue hippocampal homogenate from AD (Yao et al., 2007). This discrepancy suggests that protein or mRNA trafficking to the synapse may be altered in AD, resulting in decreased antioxidant capacity in the compartment where it is most needed. High levels of reactive oxygen species, which occur in AD nerve-endings, can damage peroxiredoxin-2 (Cumming et al., 2007).

4.5. Proteasome

Levels of proteasome complexes, Rpt1 subunits, and hyperphosphorylated *tau* are reportedly increased in AD brain synaptosomes (Tai et al., 2012). Hyperphosphorylated *tau* is highly insoluble; its aggregation induces ubiquitin immunoreactivity in AD brain (Layfield et al., 2005), which could explain the increased proteasome activity at AD synapses. We found significantly higher expression of proteasome subunit β type 6 in AD hippocampal synaptosomes when compared with those from AD motor cortex, whereas no significant difference was observed in the equivalent non-AD comparison. The ubiquitin-proteasome system may become disrupted in AD brain through overloaded or malfunctioning ubiquitinated proteins (Upadhya and Hegde, 2007). Since this system is essential for regulating the integrity of the synapse, its disturbance could lead to synaptic dysfunction.

4.6. Synaptic vesicle-related proteins

We found three synaptic vesicle-related proteins that were differentially expressed in AD brain. Synapsin-2 levels were higher in AD hippocampus than in AD motor cortex (Fig. S2), which corroborates the reported up-regulation of synapsin-2 in a transgenic mouse model of AD (David et al., 2006). Higher expression may be part of a compensatory mechanism for the loss of synaptic endings and the deterioration in neurotransmission. Vesicle amine transport 1 expression was significantly higher in non-AD hippocampus than in non-AD motor cortex but AD hippocampus and AD motor cortex did not differ. Higher expression in non-AD hippocampus compared with non-AD motor cortex may reflect a protective mechanism against age-related loss of synapses in normal aging brain that is exacerbated in AD. The vesicle-related protein zinc transporter 3 was also differentially expressed. Zinc transporter 3 mRNA expression is up to 60% lower in pathologically affected areas of AD brain (Beyer et al., 2009). In contrast, the protein level is increased in the

cortex of an AD transgenic mouse model (Zheng et al., 2010), and our study using human AD brain conforms with the latter: zinc transporter 3 expression was higher in AD hippocampus than in AD motor cortex. Higher expression would increase Zn^{2+} release into AD hippocampus synapses, accelerating plaque formation by directly binding to amyloid β (Bush et al., 1994).

4.7. Energy-related

We found significant down-regulation of oxoglutarate dehydrogenase complex component E2 in AD and non-AD hippocampus when compared with AD and non-AD motor cortices respectively, but the extent of difference was greater in AD brain. Oxoglutarate dehydrogenase activity is diminished in AD (Gibson et al., 1988). The reduction in enzyme activity could be greater than the loss of protein indicates. Reduced expression and activity at synapses would impair glutamate metabolism and probably enhance excitotoxicity-induced cell death in AD.

4.8. Unknown function

Two proteins, tryptophan-aspartic acid repeat-containing protein 37 (WDR37) and peptidyl-prolyl cis-trans isomerase-like 1 (PPIL1), both with unknown synaptic function, were differentially expressed. The expression of WDR37 was significantly lower in AD hippocampus than in AD motor cortex, but did not differ between these two areas in non-AD tissues. The function of this protein is unknown; it could be involved in various cellular processes including signal transduction, gene regulation, and apoptosis, in conformity with its family members (NCBI, 2014). PPIL1 expression was significantly higher in AD hippocampal synaptosomes than in those from AD motor cortex. Overexpression has been implicated in growth of colon cancer cells by remodeling microtubules (Obama et al., 2006). Under physiological conditions PPIL1 may a role in protein folding and pre-mRNA splicing (Xu et al., 2006); however, its function at synapses is not known.

4.9. Pathway analysis

Thirty differentially regulated synaptic proteins were further analyzed using IPA core analysis and pathway analysis. Core analysis revealed that the most affected molecular and cellular functions were cellular assembly and organization, cellular function and maintenance, cell-to-cell signaling and interaction, cell morphology, and cellular development. As expected, structural proteins including INA, NFL, NFM, neurofilament heavy polypeptide (NFH) and the septins were involved in various cellular assembly and such functions as organization of the cytoskeleton, dendritic growth/branching, and the deployment, clustering, and dissociation of neurofilaments. Structural proteins (NFH and NFM; Rao et al., 2003), adhesion molecules (contactin 2; Kamiguchi et al., 1998) and signaling proteins (RhoG; Govek et al., 2005 and versican; Wu et al., 2004) play roles in the growth of neurites. The proteins rabphilin, septin 5 and synapsin-2 are involved in the release of neurotransmitters (Dong et al., 2003; Kile et al., 2010; Tan et al., 2014). All these functions could be affected in AD hippocampus by changes in the expression of key proteins.

The top-ranked network from IPA core analysis was visualized (Fig. 3). Ubiquitin C, serine/arginine repetitive matrix 2, sirtuin 7, tubulin β-3 chain, tubulin β-4B chain, septin 9 and presenilin 1 were found to be closely associated with synaptic proteins that were differentially regulated in AD-affected areas. Ubiquitin C, a member of ubiquitin family, binds to septins 2, 5, 7, 8, 9 and 11, PPIL1, oxoglutarate dehydrogenase complex component E2, tubulin α-4A chain, tubulin β-4A chain, γ-aminobutyric acid receptor-associated protein-like 2, NADP transhydrogenase, mitochondrial, contactin 2, INA, synapsin-2, NFL, NFM and NFH. Ubiquitination is involved in various cellular functions, including endocytosis, protein degradation, kinase modification, and regulation of cell signaling pathways. It would be of value to determine whether altered levels of these proteins affect their binding to ubiquitin C, as this might result in altered functionality. Pathway analysis also showed that sirtuin 7 binds with tubulin, NFM, NFL and INA. However, the functions of human sirtuins have not yet been determined. Presenilin 1 is well known for its involvement in AD. It has a potential role in regulating the expression of tubulin polymerization-promoting protein and tubulin α-4A chain (Martin et al., 2008). Further exploration of these newly identified proteins by SWATH data mining and/or functional studies appears warranted.

In summary, we used two front-end sample-processing techniques – subcellular fractionation and SCX fractionation – with SWATH acquisition-based mass spectrometry analysis to identify over 2000 proteins in nerve endings from human AD brain. We quantified these proteins and found that 30 unique synaptic proteins were differentially expressed in AD hippocampus, including 17 novel proteins. SWATH is a relatively new technique that has room for improvement as discussed above. With improved, user-friendly data processing software, SWATH analysis will become a useful tool for studying scarce samples such as human brain. Proteins identified in this study have potential as disease markers and drug targets.

Acknowledgements

Financial support was provided by the Alzheimer's Association (USA) under grant # RG1-96-005 and the Judith Jane Mason and Harold Stannett Williams Memorial Foundation CT 21926. The Australian Brain Bank Network, of which the Queensland Brain Bank is a node, is supported by an NHMRC (Australia) Enabling Grant (N° 605210).

Appendix: Supplementary material

Supplementary data to this article can be found online at doi:10.1016/j.neuint.2015.04.004.

References

Andreev, V.P., Petyuk, V.A., Brewer, H.M., Karpievitch, Y.V., Xie, F., Clarke, J., et al., 2012. Label-free quantitative LC-MS proteomics of Alzheimer's disease and normally aged human brains. J. Proteome Res. 11, 3053–3067.
Baeriswyl, T., Stoeckli, E.T., 2008. Axonin-1/TAG-1 is required for pathfinding of granule cell axons in the developing cerebellum. Neural Develop. 3, 7.
Baum, L.W., 2005. Sex, hormones, and Alzheimer's disease. J. Gerontol. A. Biol Sci. Med Sci 60, 736–743.
Beites, C.L., Campbell, K.A., Trimble, W.S., 2005. The septin Sept5/CDCrel-1 competes with α-SNAP for binding to the SNARE complex. Biochem. J. 385, 347–353.
Beyer, N., Coulson, D.T., Heggarty, S., Ravid, R., Irvine, G.B., Hellemans, J., et al., 2009. ZnT3 mRNA levels are reduced in Alzheimer's disease post-mortem brain. Mol. Neurodegener. 4, 53.
Buggia-Prévot, V., Fernandez, C.G., Udayar, V., Vetrivel, K.S., Elie, A., Roseman, J., et al., 2013. A function for EHD family proteins in unidirectional retrograde dendritic transport of BACE1 and Alzheimer's disease A® production. Cell Rep. 5, 1552–1563.
Bush, A.I., Pettingell, W.H., Multhaup, G., d Paradis, M., Vonsattel, J.P., Gusella, J.F., et al., 1994. Rapid induction of Alzheimer A® amyloid formation by zinc. Science 265, 1464–1467.
Chang, R.Y.K., Nouwens, A.S., Dodd, P.R., Etheridge, N., 2013. The synaptic proteome in Alzheimer's disease. Alzheimers Dement. 9, 499–511.
Chang, R.Y.K., Etheridge, N., Dodd, P.R., Nouwens, A.S., 2014a. Quantitative multiple reaction monitoring analysis of synaptic proteins from human brain. J. Neurosci. Methods 227, 189–210.
Chang, R.Y.K., Etheridge, N., Dodd, P.R., Nouwens, A.S., 2014b. Targeted quantitative analysis of synaptic proteins in Alzheimer's disease brain. Neurochem. Int. 75, 66–75.
Chin, L.S., Nugent, R.D., Raynor, M.C., Vavalle, J.P., Li, L., 2000. SNIP, a novel SNAP-25-interacting protein implicated in regulated exocytosis. J. Biol. Chem. 275, 1191–1200.
Collins, B.C., Gillet, L.C., Rosenberger, G., Rost, H.L., Vichalkovski, A., Gstaiger, M., et al., 2013. Quantifying protein interaction dynamics by SWATH mass spectrometry: application to the 14-3-3 system. Nat. Methods 10, 1246–1253.

Cumming, R.C., Dargusch, R., Fischer, W.H., Schubert, D., 2007. Increase in expression levels and resistance to sulfhydryl oxidation of peroxiredoxin isoforms in amyloid β-resistant nerve cells. J. Biol. Chem. 282, 30523–30534.
David, D.C., Ittner, L.M., Gehrig, P., Nergenau, D., Shepherd, C., Halliday, G., et al., 2006. ®-Amyloid treatment of two complementary P301L tau-expressing Alzheimer's disease models reveals similar deregulated cellular processes. Proteomics 6, 6566–6577.
Deak, F., Shin, O.H., Tang, J., Hanson, P., Ubach, J., Jahn, R., et al., 2006. Rabphilin regulates SNARE-dependent re-priming of synaptic vesicles for fusion. EMBO J. 25, 2856–2866.
DeKosky, S.T., Scheff, S.W., 1990. Synapse loss in frontal cortex biopsies in Alzheimer's disease: correlation with cognitive severity. Ann. Neurol. 27, 457–464.
Dodd, P.R., Hardy, J.A., Oakley, A.E., Edwardson, J.A., Perry, E.K., Delaunoy, J.P., 1981. A rapid method for preparing synaptosomes: comparison with alternative procedures. Brain Res. 226, 107–118.
Dong, Z., Ferger, B., Paterna, J.C., Vogel, D., Furler, S., Osinde, M., et al., 2003. Dopamine-dependent neurodegeneration in rats induced by viral vector-mediated overexpression of the parkin target protein, CDCrel-1. Proc. Natl. Acad. Sci. U.S.A. 100, 12438–12443.
Dours-Zimmermann, M.T., Maurer, K., Rauch, U., Stoffel, W., Fassler, R., Zimmermann, D.R., 2009. Versican V2 assembles the extracellular matrix surrounding the nodes of Ranvier in the CNS. J. Neurosci. 29, 7731–7742.
Etheridge, N., Lewohl, J.M., Mayfield, R.D., Harris, R.A., 2009. Synaptic proteome changes in the superior frontal gyrus and occipital cortex of the alcoholic brain. Proteomics Clin. Appl. 3, 730–742.
Gautam, V., D'Avanzo, C., Hebisch, M., Kovacs, D.M., Kim, D.Y., 2014. BACE1 activity regulates cell surface contactin-2 levels. Mol. Neurodegener. 9, 4.
Gibson, G.E., Sheu, K.F., Blass, J.P., Baker, A., Carlson, K.C., Harding, B., et al., 1988. Reduced activities of thiamine-dependent enzymes in the brains and peripheral tissues of patients with Alzheimer's disease. Arch. Neurol. 45, 836–840.
Gillet, L.C., Navarro, P., Tate, S., Rost, H., Selevsek, N., Reiter, L., et al., 2012. Targeted data extraction of the MS/MS spectra generated by data-independent acquisition: a new concept for consistent and accurate proteome analysis. Mol. Cell. Proteomics 11, O111.016717.
Govek, E.E., Newey, S.E., Van Aelst, L., 2005. The role of the Rho GTPases in neuronal development. Genes Devel. 19, 1–49.
Grant, S.G., 2006. The synapse proteome and phosphoproteome: a new paradigm for synapse biology. Biochem. Soc. Trans. 34, 59–63.
Haverland, N.A., Fox, H., Ciborowski, P., 2014. Quantitative proteomics by SWATH-MS reveals altered expression of nucleic acid binding and regulatory proteins in HIV-1-infected macrophages. J. Proteome Res. 13, 2109–2119.
Honer, W.G., Dickson, D.W., Gleeson, J., Davies, P., 1992. Regional synaptic pathology in Alzheimer's disease. Neurobiol. Aging 13, 375–382.
Ito, H., Atsuzawa, K., Sudo, K., Di Stefano, P., Iwamoto, I., Morishita, R., et al., 2008. Characterization of a multidomain adaptor protein, p140Cap, as part of a pre-synaptic complex. J. Neurochem. 107, 61–72.
Kamiguchi, H., Hlavin, M.L., Yamasaki, M., Lemmon, V., 1998. Adhesion molecules and inherited diseases of the human nervous system. Annu. Rev. Neurosci. 21, 97–125.
Kile, B.M., Guillot, T.S., Venton, B.J., Wetsel, W.C., Augustine, G.J., Wightman, R.M., 2010. Synapsins differentially control dopamine and serotonin release. J. Neurosci. 30, 9762–9770.
Kittur, S., Hoh, J., Endo, H., Tourtellotte, W., Weeks, B.S., Markesbery, W., et al., 1994. Cytoskeletal neurofilament gene expression in brain tissue from Alzheimer's disease patients. I. Decrease in NF-L and NF-M message. J. Geriatr. Psychiatry Neurol. 7, 153–158.
Layfield, R., Lowe, J., Bedford, L., 2005. The ubiquitin-proteasome system and neurodegenerative disorders. Essays Biochem. 41, 157–171.
Li, X., Serwanski, D.R., Miralles, C.P., Nagata, K., De Blas, A.L., 2009. Septin 11 is present in GABAergic synapses and plays a functional role in the cytoarchitecture of neurons and GABAergic synaptic connectivity. J. Biol. Chem. 284, 17253–17265.
Martin, B., Brenneman, R., Becker, K.G., Gucek, M., Cole, R.N., Maudsley, S., 2008. iTRAQ analysis of complex proteome alterations in 3xTgAD Alzheimer's mice: understanding the interface between physiology and disease. PLoS ONE 3, e2750.
Mathieu-Kia, A.M., Fan, L.Q., Kreek, M.J., Simon, E.J., Hiller, J.M., 2001. μ-, ™- and (-Opioid receptor populations are differentially altered in distinct areas of postmortem brains of Alzheimer's disease patients. Brain Res. 893, 121–134.
NCBI, 2014. WDR37 WD repeat domain 37 [*Homo sapiens* (human)] National Center for Biotechnology Information.
Obama, K., Kato, T., Hasegawa, S., Satoh, S., Nakamura, Y., Furukawa, Y., 2006. Overexpression of peptidyl-prolyl isomerase-like 1 is associated with the growth of colon cancer cells. Clin. Cancer Res. 12, 70–76.
Rao, M.V., Campbell, J., Yuan, A., Kumar, A., Gotow, T., Uchiyama, Y., et al., 2003. The neurofilament middle molecular mass subunit carboxyl-terminal tail domains is essential for the radial growth and cytoskeletal architecture of axons but not for regulating neurofilament transport rate. J. Cell Biol. 163, 1021–1031.
Ren, X., Rizavi, H.S., Khan, M.A., Bhaumik, R., Dwivedi, Y., Pandey, G.N., 2014. Alteration of cyclic-AMP response element binding protein in the postmortem brain of subjects with bipolar disorder and schizophrenia. J. Affect. Disord. 152–154, 326–333.
Rivera-Gines, A., Cook, R.J., Loh, H.H., Ko, J.L., 2006. Interplay of Sps and poly(C) binding protein 1 on the μ-opioid receptor gene expression. Biochem. Biophys. Res. Commun. 345, 530–537.
Savvaki, M., Panagiotaropoulos, T., Stamatakis, A., Sargiannidou, I., Karatzioula, P., Watanabe, K., et al., 2008. Impairment of learning and memory in TAG-1 deficient mice associated with shorter CNS internodes and disrupted juxtaparanodes. Mol. Cell. Neurosci. 39, 478–490.
Schmalfeldt, M., Dours-Zimmermann, M.T., Winterhalter, K.H., Zimmermann, D.R., 1998. Versican V2 is a major extracellular matrix component of the mature bovine brain. J. Biol. Chem. 273, 15758–15764.
Shi, M., Jin, J., Wang, Y., Beyer, R.P., Kitsou, E., Albin, R.L., et al., 2008. Mortalin: a protein associated with progression of Parkinson disease? J. Neuropathol. Exp. Neurol. 67, 117–124.
Tada, T., Simonetta, A., Batterton, M., Kinoshita, M., Edbauer, D., Sheng, M., 2007. Role of septin cytoskeleton in spine morphogenesis and dendrite development in neurons. Curr. Biol. 17, 1752–1758.
Tai, H.C., Serrano-Pozo, A., Hashimoto, T., Frosch, M.P., Spires-Jones, T.L., Hyman, B.T., 2012. The synaptic accumulation of hyperphosphorylated tau oligomers in Alzheimer disease is associated with dysfunction of the ubiquitin-proteasome system. Am. J. Pathol. 181, 1426–1435.
Takano, M., Yamashita, T., Nagano, K., Otani, M., Maekura, K., Kamada, H., et al., 2013. Proteomic analysis of the hippocampus in Alzheimer's disease model mice by using two-dimensional fluorescence difference in gel electrophoresis. Neurosci. Lett. 534, 85–89.
Tan, M.G.K., Lee, C., Lee, J.H., Francis, P.T., Williams, R.J., Ramírez, M.J., et al., 2014. Decreased rabphilin 3A immunoreactivity in Alzheimer's disease is associated with Aβ burden. Neurochem. Int. 64, 29–36.
Tremblay, C., St-Amour, I., Schneider, J., Bennett, D.A., Calon, F., 2011. Accumulation of transactive response DNA binding protein 43 in mild cognitive impairment and Alzheimer disease. J. Neuropathol. Exp. Neurol. 70, 788–798.
Upadhya, S.C., Hegde, A.N., 2007. Role of the ubiquitin proteasome system in Alzheimer's disease. BMC Biochem. 8 (Suppl. 1), S12.
Wu, Y., Sheng, W., Chen, L., Dong, H., Lee, V., Lu, F., et al., 2004. Versican V1 isoform induces neuronal differentiation and promotes neurite outgrowth. Mol. Biol. Cell 15, 2093–2104.
Xu, C., Zhang, J., Huang, X., Sun, J., Xu, Y., Tang, Y., et al., 2006. Solution structure of human peptidyl prolyl isomerase-like protein 1 and insights into its interaction with SKIP. J. Biol. Chem. 281, 15900–15908.
Yao, J., Taylor, M., Davey, F., Ren, Y., Aiton, J., Coote, P., et al., 2007. Interaction of amyloid binding alcohol dehydrogenase/Aβ mediates up-regulation of peroxiredoxin II in the brains of Alzheimer's disease patients and a transgenic Alzheimer's disease mouse model. Mol. Cell. Neurosci. 35, 377–382.
Zheng, W., Wang, T., Yu, D., Feng, W.Y., Nie, Y.X., Stoltenberg, M., et al., 2010. Elevation of zinc transporter ZnT3 protein in the cerebellar cortex of the AβPP/PS1 transgenic mouse. J. Alzheimers Dis. 20, 323–331.
Zhou, J., Jones, D.R., Duong, D.M., Levey, A.I., Lah, J.J., Peng, J., 2013. Proteomic analysis of postsynaptic density in Alzheimer's Disease. Clin. Chim. Acta 420, 62–68.